



Multiscale simulations of charge and size separation of nanoparticles with a solid-state nanoporous membrane

Craig C. Wells, Dmitriy V. Melnikov, Joshua T. Cirillo , and Maria E. Gracheva *

Department of Physics, Clarkson University, Potsdam, New York 13699, USA



(Received 18 June 2020; accepted 19 November 2020; published 10 December 2020)

Nanoporous membranes provide an attractive approach for rapid filtering of nanoparticles at high-throughput volume, a goal useful to many fields of science and technology. Creating a device to readily separate different particles would require an extensive knowledge of particle-nanopore interactions and particle translocation dynamics. To this end, we use a multiscale model for the separation of nanoparticles by combining microscopic Brownian dynamics simulations to simulate the motion of spherical nanoparticles of various sizes and charges in a system with nanopores in an electrically biased membrane with a macroscopic filtration model accounting for bulk diffusion of nanoparticles and membrane surface pore density. We find that, in general, the separation of differently sized particles is easier to accomplish than of differently charged particles. The separation by charge can be better performed in systems with low pore density and/or smaller filtration chambers when electric nanopore-particle interactions are significant. The results from these simple cases can be used to gain insight in the more complex dynamics of separating, for example, globular proteins.

DOI: [10.1103/PhysRevE.102.063104](https://doi.org/10.1103/PhysRevE.102.063104)

I. INTRODUCTION

The efficient separation of nanoparticles and other nano-sized objects such as proteins have been a topic of significant interest as its development can lead to advancements in methods for rapid particle filtration [1–6]. Application of membrane and nanopore-based technologies for this purpose have been the focus of many studies [7–11], for example, the effectiveness of using an electrically tunable silicon membrane as an ionic filter, as studied by Vidal *et al.* [12]. This is because nanoporous membranes have the possibility of supporting fast, large-throughput particle separation desired, for example, for commercial protein filtration. Nanopores, often created in solid-state membranes, can be fabricated with specific pore size and length appropriate for a particular application [13–17]. The nanoporous membrane is usually submerged in a container filled with an electrolyte solution, which divides it into the *cis* and *trans* chambers with particles initially added to the *cis* side as to translocate the membrane via the nanopore to the *trans* chamber.

There are many techniques that are used to encourage translocation of particles, such as applying an electric potential difference between the chambers to produce a driving force for ionic and charged particle movement through nanopores [7,18,19], applying an external pressure gradient [20–22], or through electroosmosis [23–25]. However, for the purpose of filtering particles of similar size and charge, these techniques may not lead to efficient and fast particle separation as all particles may move to the *trans* chamber from the *cis* too quickly. Some studies emphasize particle

selectivity when developing their nanopores and techniques for particle translocation [26,27]. A desirable environment will encourage the rapid translocation of one type of particle while discouraging others. Therefore, systems such as ones utilizing an electrically active semiconductor membrane are of interest as an electric bias can also be applied to the membrane. In this way, the electric potential landscape in the vicinity of the membrane and in the pore can be tuned to encourage or limit the translocation of specific particles depending on their size and charge. Alternatively, the electric potential can be changed by putting different charges on the membrane surface.

Computational modeling of particle motion has been used to discover, develop, and explain the dynamics of nanoparticle nanopore translocation [28–31]. This is done to facilitate a further insight into the difficult-to-access particle translocation characteristics produced by experimental investigations. Detailed models of a protein that include its atomic structure can in principle yield a better understanding of what is occurring on the atomic level [29,32]. On the other hand, simpler proteins models such as coarse-grained models [30,33–36] or spherical particle models [35] can be used to gain a statistical perspective on translocation dynamics while being less computationally costly. This data can then be used to describe a system on a macroscopic scale [4,37].

In this paper, we set up a multiscale model to study the ability of a nanopore separating spherical nanoparticles of different sizes and charges. The translocation dynamics of two interacting nanoparticles modeled as spherical beads is explored via a Brownian dynamics model. Additionally, each bead's size and charge is varied to determine what will facilitate filtering best. The electrostatic environment is also considered, since an electric potential applied to a nanoporous membrane can alter a nanoparticle's motion [35,37,38]. We

*Author to whom correspondence should be addressed: gracheva@clarkson.edu

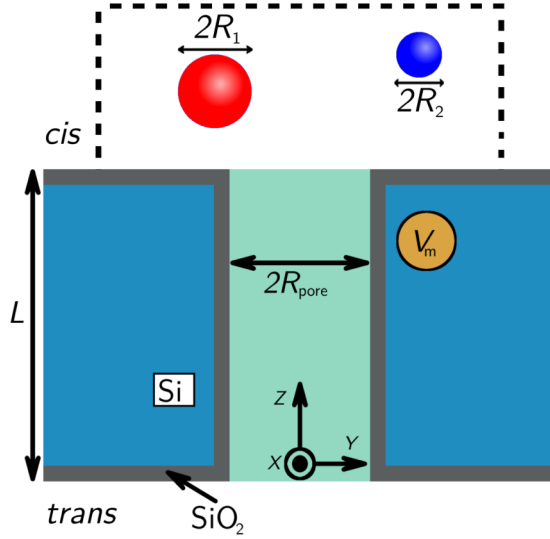


FIG. 1. Schematic diagram of the simulated system (not to scale). The Si membrane has an applied bias of $V_m = \pm 1$ V and is covered in a layer of negatively charged SiO_2 . Particle movement in the *cis* chamber is restricted by a bounding box (dashed lines above the pore). The x , y , and z axes originate at the bottom, center of the pore.

then use the data obtained from the microscopic nanoparticle translocations to develop a diffusion model [4,37], thus gaining insight on separation characteristics with macroscopically large fluid chambers. We use BD to describe translocation of particles through the nanopore to obtain the membrane resistance for our nanopore system, which is then used to develop the macroscopic diffusion model.

This paper is organized as follows. The modeled system and computational model are described in Sec. II. The results of simulations are discussed in Sec. III and in the Appendix. Our findings are summarized in Sec. IV.

II. METHOD

In this work, we consider a silicon membrane coated by a surface layer of SiO_2 , which is 8 \AA thick and has a volume charge density $\rho_{\text{SiO}_2} = -4 \times 10^{20} e/\text{cm}^3$ (corresponding to surface charge density of $3.2 \times 10^{13} e/\text{cm}^2$). A potential of $V_m = \pm 1$ V is applied to the membrane as schematically shown in Fig. 1 where $V_m = +1$ V corresponds to a positive effective surface charge while $V_m = -1$ V corresponds to a negative effective surface charge. The $L = 260 \text{ \AA}$ thick membrane separates the *cis* chamber, where nanoparticles are initially placed, from the *trans* chamber. Both chambers are filled with an aqueous KCl electrolyte solution of bulk concentration $C_{\text{KCl}} = 0.1$ M and the system's electrostatic environment $\phi(\mathbf{r}_i)$ is simulated numerically with the coupled Poisson and Nernst-Planck (PNP) equations as described in Appendix A and previous work [37–41]. The electrolyte bias is held at zero across the membrane ($V_e = 0$).

The *cis* chamber is connected to the *trans* chamber via a nanopore, where its radius is varied from $R_{\text{pore}} = 34 \text{ \AA}$ to 60 \AA . A bounding box of radius 100 \AA and height 130 \AA confines the motion of beads within the *cis* chamber, giving

rise to a particle concentration of ~ 0.8 mM when there are two beads considered per box, corresponding to potentially applicable biological systems as explored in Refs. [31,35]. The *trans* chamber does not have a bounding box such that the beads can move away from the nanopore. This simulates the effect of having a low particle concentration in the *trans* chamber at all times. A simulation begins after two beads are positioned randomly within the bounding box and ends when both have moved into the *trans* chamber.

The movement of particles is simulated using Brownian dynamics (BD), similar to our previous studies [35,41,42]. Using this approach, the i th particle's (radius R_i , charge q_i) center of mass position \mathbf{r}_i at time t is determined using

$$\mathbf{r}_i(t) = \mathbf{r}_i(t - \delta t) - \nabla_i U[\mathbf{r}_i(t - \delta t)] \frac{\delta t}{\xi_i} + \sqrt{\frac{6\delta t k_b T}{\xi_i}} \mathbf{n},$$

$$i = 1, 2, \quad (1)$$

where $\delta t = 1.0$ ps is the time step. In Eq. (1) the second term corresponds to the net external force applied to the bead determined by $U(\mathbf{r}_i) = U_b + U_m + U_C + q_i \phi(\mathbf{r}_i)$ where $U_{b,m} = \epsilon_{b,m} [(\sigma_{b,m}/r_{b,m})^{12} - 2(\sigma_{b,m}/r_{b,m})^6]$ is the bead-bead or bead-membrane Lennard-Jones (LJ) interaction, $U_C = (4\pi \epsilon_0 \epsilon_r^{\text{KCl}})^{-1} q_1 q_2 \exp(-r_b/L_D)/r_b$ is the screened Coulomb interaction between particles, and $q_i \phi(\mathbf{r}_i)$ is the electric potential energy [31]. In these energies, $\epsilon_{b,m} = 0.1$ kcal/mol, $\sigma_b = 5 \text{ \AA}$, $\sigma_m = 2.5 \text{ \AA}$ corresponding with our previous protein studies [31,35], $r_{b,m}$ is the distance between the bead's surface and the other bead's surface or membrane surface, relative permittivity of the KCl electrolyte solution $\epsilon_r^{\text{KCl}} = 78$, and Debye screening length $L_D = 0.96$ nm. The last term in Eq. (1) is the random force responsible for stochastic motion of the bead where $T = 300$ K and \mathbf{n} is the three-dimensional (3D) random vector with components uniformly distributed in $[-1, 1]$ [31,43,44]. An example of a single simulation showing trajectories of two particles is presented in Fig. 2.

Stokes formula $\xi_i = 6\pi \eta R_i$, where $\eta = 10^{-3} \text{ Pa} \cdot \text{s}$ is the solution viscosity, is used to approximate the drag coefficient for the spherical particle in the bulk away from the membrane surface and nanopore. While the particle is within the nanopore, its movement is impeded due to the hindered diffusion effect, which accounts for a decrease in diffusion coefficient with increasing ratio R_i/R_{pore} [45], resulting in a larger drag coefficient in Eq. (1) when compared to the drag coefficient in the bulk. The drag coefficient outside of the pore as the particle approaches the membrane surface is approximately proportional to $\sim (1 - R_i/h)^{-1}$ where h is the perpendicular distance the particle is from the surface [46]. The drag coefficient is linearly interpolated between the value when the particle is closest to the outer membrane surface and the value of the drag inside the nanopore.

Since the particle's drag coefficient is position dependent, an additional term in Eq. (1) $\sim (k_b T) \nabla \cdot (1/\xi_i)$ [47,48] should be taken into account. However, in this work said term results in a particle's movement ranging from 10^{-4} - 10^{-6} \AA per time step. This is considerably smaller than the particle movement per time step from the external forces and stochastic term, which are $\sim 0.2 \text{ \AA}$. As such, this term is omitted from Eq. (1).

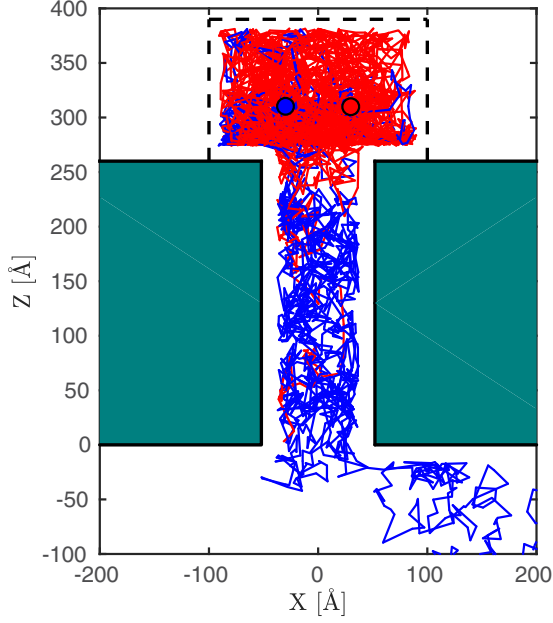


FIG. 2. Particle traces over the course of a single simulation ($R_{\text{pore}} = 52 \text{ \AA}$, $V_m = 1 \text{ V}$, $R_1 = R_2 = 10 \text{ \AA}$, $q_1 = q_2 = -5e$). Both beads begin in the *cis* chamber and move according to Eq. (1) until both particles have translocated the nanopore to the *trans* chamber where there is no bounding box restricting movement.

From simulating the BD motion of a spherical bead, we calculate its waiting time t_w , the time from the beginning of the simulation to when the molecule enters the pore prior to its successful translocation into the *trans* chamber ($z = 0 \text{ \AA}$). The average of these waiting times for a given set of parameters, $\langle t_w \rangle$, indicates effectiveness of separating different particles using a nanopore, where larger differences in $\langle t_w \rangle$ imply better separation [37].

When studying the separation of particles macroscopically, we then use the average waiting time to define the effective resistance of the membrane $\Omega_m = \langle t_w \rangle / NV_b$, where N is the area density of the pores and V_b is the volume of the bounding box in the BD simulations [37]. This membrane resistance accounts for macroscopic pore discovery and transmembrane permeability via the average waiting time of the BD model results. The concentration of nanoparticles of a given kind, $c(z, t)$, is determined by solving the one-dimensional diffusion equation along the nanopore axis:

$$\frac{\partial c_i}{\partial t} = \frac{k_B T}{\xi_i} \frac{\partial^2 c_i}{\partial z^2}, \quad i = 1, 2, \quad -AW_1 = -W_2 < z < W_1, \quad (2)$$

where the *cis* chamber's length is W_1 and the *trans* chamber's length is $W_2 = AW_1$ where $A \gg 1$ in order to ensure all particles end up in the *trans* chamber. Initially, all nanoparticles are located in the *cis* chamber ($z > 0$), so that $c_i(z > 0, t = 0) = c_{0i}$ and $c_i(z < 0, t = 0) = 0$.

To describe the macroscopic diffusion of particles from the *cis* chamber toward and through the membrane, the effective resistance of the fluid to the flow of particles is also taken into account. The fluid resistance of a chamber of length W_1 to

the flow of nanoparticles is given by $\Omega_{ci} = \xi_i W_1 / k_B T$ [4]. The ratio of Ω_c and Ω_m , denoted as β , is

$$\beta_i = \frac{\Omega_{mi}}{\Omega_{ci}} = \frac{\langle t_w \rangle_i k_B T}{NV_b \xi_i W_1}. \quad (3)$$

Since the membrane thickness is much smaller than the size of the *cis* chamber, the concentration change across the membrane at $z = 0$ can be written as

$$\frac{k_B T}{\xi_i} \frac{\partial c_i}{\partial z} \Big|_{z=0} = \Omega_{mi}^{-1} [c_i(+0, t) - c_i(-0, t)]. \quad (4)$$

The solution to the above boundary-value problem given by Eqs. (2)–(4) can be written as

$$c_i(z, t) = c_{0i} \left[\frac{1}{1+A} + \sum_{n=0}^{\infty} a_n \chi_n(z) \exp\left(-\frac{k_B T \lambda_n^2 t}{\xi_i W_1^2}\right) \right], \quad (5)$$

where

$$a_n = \frac{4 \sin(\lambda_n)}{2\lambda_n(1+A\alpha^2) + \sin(2\lambda_n) + \alpha^2 \sin(2A\lambda_n)}, \quad (6)$$

$$\alpha = \frac{\sin(\lambda_n)}{\sin(A\lambda_n)}, \quad (7)$$

$$\chi_n = \begin{cases} \cos(\lambda_n(W_1 - z)/W_1), & 0 < z < W_1, \\ -\alpha \cos(\lambda_n(W_2 + z)/W_1), & -W_2 < z < 0, \end{cases} \quad (8)$$

and eigenvalues λ_n are determined from solutions of

$$\frac{\sin(\lambda_n) \sin(A\lambda_n)}{\sin((1+A)\lambda_n)} = \frac{1}{\beta_i \lambda_n}. \quad (9)$$

From Eqs. (5)–(9), we calculate the average concentration in the *cis* chamber $c_{ci}(t)$, which we use to define the macroscopic translocation probability,

$$P_{Ti}^c(t) = 1 - c_{ci}(t)/c_{0i}, \quad i = 1, 2. \quad (10)$$

The translocation probability for particles $i = 1, 2$ are then compared to infer the viability of particle separation, where larger differences in P_{Ti}^c would lead to greater separation. In practice, these probabilities correspond to, for example, fluorescence intensities of translocated objects vs. time as measured by Striemer *et al.* [2].

III. RESULTS AND DISCUSSION

A. Separation of two differently sized or charged particles

To determine the effectiveness of using nanoporous membranes for high-throughput filtering, simulations of two different nanoparticles were performed. In these scenarios, beads of different (same) radii of 10 \AA and 20 \AA with the same (different) electric charge of $-5e$ and $0e$ are considered. The data from ~ 2000 simulations were used to find the average waiting time $\langle t_w \rangle$ for both particles in the system. Using this time, the probability that a particle has translocated the nanopore in time t , P_T , can be written as

$$P_T(t) = 1 - \exp(-t/\langle t_w \rangle), \quad (11)$$

so that, in a case where there are two different types of particles, the difference between their translocation probabilities

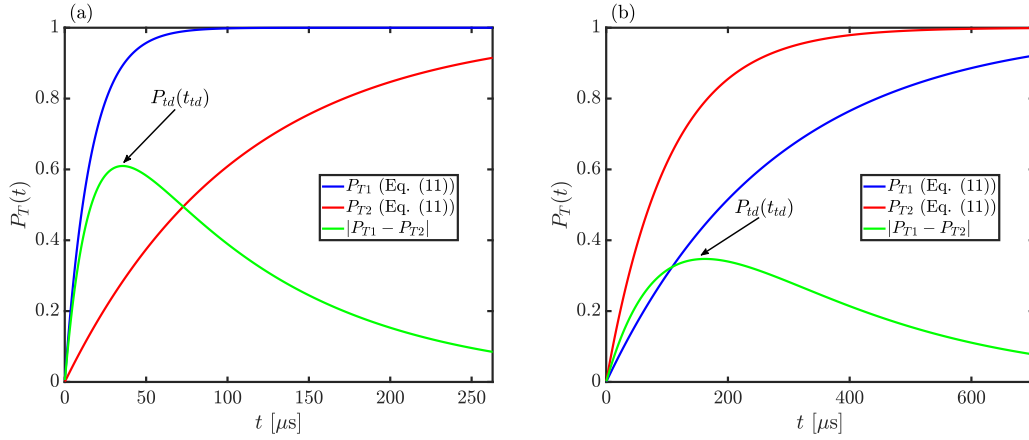


FIG. 3. Probability that a bead translocates the nanopore, P_{T1} and P_{T2} , vs time t in a system where $R_{\text{pore}} = 34 \text{ \AA}$ and (a) $V_m = 1 \text{ V}$, $R_1 = 10 \text{ \AA}$, $R_2 = 20 \text{ \AA}$, $q_1 = q_2 = -5e$ and (b) $V_m = 1 \text{ V}$, $q_1 = 0 \text{ e}$, $q_2 = -5e$, $R_1 = R_2 = 20 \text{ \AA}$. The difference of translocation probability $|P_{T1} - P_{T2}|$ is also calculated, the peak of which, P_{Id} , indicates the maximum extent of bead separation that will occur in the system at peak translocation probability difference time t_{Id} .

indicates how effective the separation can be. A detailed discussion on how t_w depends on various parameters is given in the Appendix B.

The translocation probabilities and their difference for two particles are shown for two cases in Fig. 3 where the peak of the difference is referred to as P_{Id} and time at which it happens is t_{Id} . The most favorable circumstances for filtration is a large value of P_{Id} that occurs at the shortest time t_{Id} , since that represents high-throughput, large percent separation of nanoparticles. In Fig. 3(a), the translocation probabilities and their differences for $R_1 = 10 \text{ \AA}$, $R_2 = 20 \text{ \AA}$, $q_{1,2} = -5e$, $V_m = 1 \text{ V}$, and $R_{\text{pore}} = 34 \text{ \AA}$ are shown, which is one of the best separation scenarios studied. As it is seen, the likelihood of the $R_1 = 10 \text{ \AA}$ particle translocating the nanopore first is much greater than that of the larger particle. The difference in their probabilities peak at $P_{Id} \sim 0.60$. This is the same as saying the maximum percentage difference between two types of particles in either chamber is $\sim 60\%$.

On the other hand, Fig. 3(b) shows the translocation probability of $R_{1,2} = 20 \text{ \AA}$ particles with different electric charges $q_1 = 0$ and $q_2 = -5e$. P_{Id} occurs at larger times and is smaller than that shown in Fig. 3(a). We can conclude that the separation is less effective for beads of the same size but different charges in this nanoporous membrane system.

The value of P_{Id} for all cases investigated vs. the pore radius R_{pore} with its corresponding t_{Id} is shown in Fig. 4. For all cases, P_{Id} decreases as the pore size increases, including the cases when the two simulated beads have a different charge but the same radius. The highest P_{Id} at the lowest time t_{Id} are found for separating $R_1 = 10 \text{ \AA}$, $q_1 = -5e$ particles from $R_2 = 20 \text{ \AA}$, $q_2 = -5e$ particles at $V_m = 1 \text{ V}$. This is due to the ease at which smaller particles find and access the nanopore, along with having a reduced drag. In general, a $V_m = 1 \text{ V}$ bias results in a higher P_{Id} for separating negatively charged particles of different sizes with smaller t_{Id} , a result that is followed closely by neutral particles of different sizes. Separation of negative particles of different sizes at $V_m = -1 \text{ V}$ yields much larger t_{Id} than the other two cases. This suggests that when separating two particles of different sizes but same charge, it is best to attract the particles to the membrane in order for

them to find the nanopore entrance faster since it will lead to separation in a shorter time, and thus, a higher throughput.

For any given R_{pore} , the smallest P_{Id} values, and therefore hardest to separate particles, correspond to particles of the same size but different charge with results being approximately the same for $V_m = 1 \text{ V}$ and $V_m = -1 \text{ V}$. Because of this, peak time t_{Id} would determine which system would be more favorable for filtration. One can see in Fig. 4 that t_{Id} for $V_m = -1 \text{ V}$ is always larger than when $V_m = 1 \text{ V}$. This is because it is more time efficient to attract a negatively charged particle to the nanopore at $V_m = 1 \text{ V}$ before a neutral particle manages to translocate a pore rather than repel the charged particle from it to allow a neutral one to translocate first.

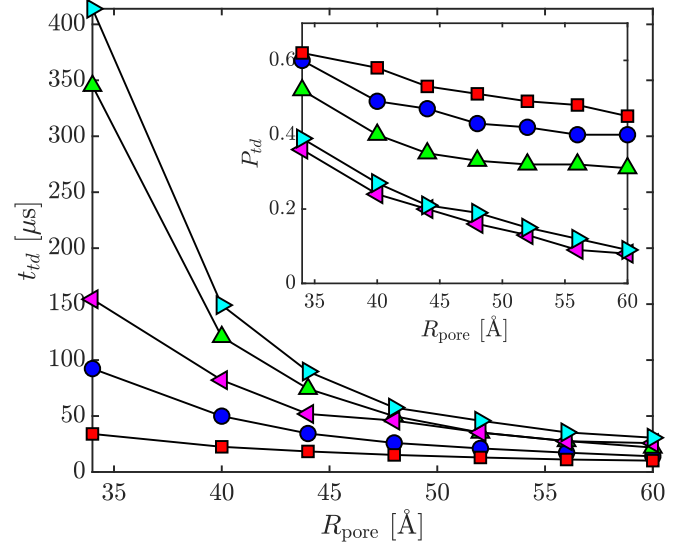


FIG. 4. Peak translocation probability difference time t_{Id} and (inset) the maximum translocation probability difference P_{Id} for a system where (○) $R_1 = 10 \text{ \AA}$, $R_2 = 20 \text{ \AA}$, $q_i = 0$; (□) $V_m = 1 \text{ V}$, $R_1 = 10 \text{ \AA}$, $R_2 = 20 \text{ \AA}$, $q_i = -5e$; (△) $V_m = -1 \text{ V}$, $R_1 = 10 \text{ \AA}$, $R_2 = 20 \text{ \AA}$, $q_i = -5e$; (<) $V_m = 1 \text{ V}$, $q_1 = -5e$, $q_2 = 0$, $R_i = 20 \text{ \AA}$; (▷) $V_m = -1 \text{ V}$, $q_1 = 0$, $q_2 = -5e$, $R_i = 20 \text{ \AA}$.

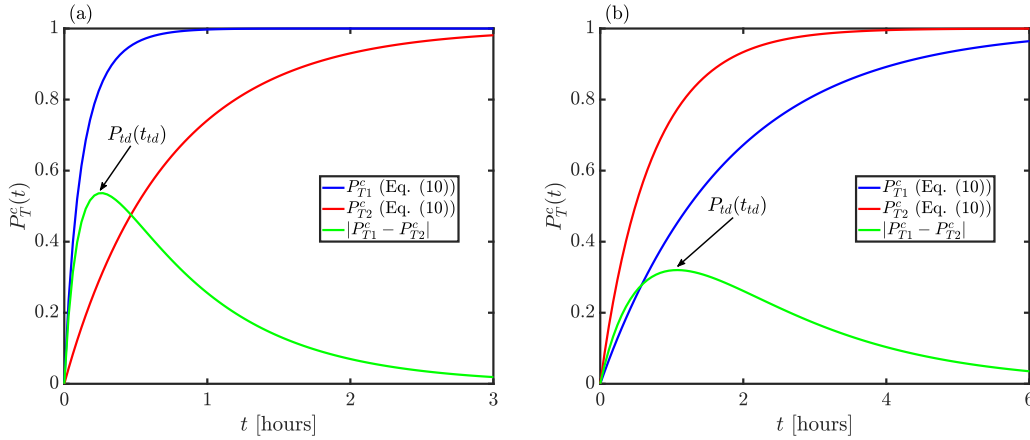


FIG. 5. Probability that a bead translocates the nanopore, P_{T1}^c and P_{T2}^c , vs time t in a system where $R_{\text{pore}} = 34 \text{ \AA}$ (a) $V_m = 1 \text{ V}$, $R_1 = 10 \text{ \AA}$, $R_2 = 20 \text{ \AA}$, $q_1 = q_2 = -5e$ and (b) $V_m = 1 \text{ V}$, $q_1 = 0 \text{ e}$, $q_2 = -5e$, $R_1 = R_2 = 20 \text{ \AA}$. For Eqs. (5)–(9), $N = 10^8 \text{ cm}^{-2}$, $W_1 = 0.1 \text{ mm}$, and $W_2 = 10W_1$. The difference of translocation probability $|P_{T1}^c - P_{T2}^c|$ is also calculated where P_{td} is its peak value occurring at time t_{td} .

B. Macroscopic nanoparticle filtration

We next use the data of the preceding section to determine macroscopic filtration probabilities and times, as demonstrated in Fig. 5 for the same two cases as in Fig. 3. One can see that the values of t_{td} are now measured in hours rather than μs as expected due to macroscopically large sizes of the simulated filtering system while unexpectedly P_{td} values are only somewhat decreased.

Figure 6 summarizes our results for different pore densities N and chamber sizes. In Fig. 6(a) where $N = 10^6 \text{ cm}^{-2}$, $W_1 = 0.1 \text{ mm}$, and $W_2 = 10W_1$, the maximum P_{td} values are only slightly lower compared to values calculated from the microscopic simulations shown in Fig. 4.

Increasing the pore density will decrease the time it takes to reach maximum separation, as displayed in Fig. 6(b) when $N = 10^8 \text{ cm}^{-2}$. This does have consequences, however, as the peak value P_{td} compared to single-particle values in Fig. 4 is decreased at large pore density N . The trend of decreasing P_{td} also occurs when the sizes of the chambers are increased, as seen in Fig. 6(c). We found that large chamber, high pore density systems ($W_1 = 1 \text{ mm}$ and $N = 10^8 \text{ pores/cm}^2$) have values of P_{td} decreased by 10–80% compared to results of individual particle simulations in Sec. III A. Additionally, this maximum separation of the nanoparticles would take 2–29 h to reach.

When the particle concentration decreases in the region around the membrane on the *cis* side quickly (see Fig. 7 where concentration profiles along the z direction are shown for different filtration times) relative to the concentration in the bulk, then the increase of particle concentration in the *trans* chamber is largely determined by how long it takes for the concentration near the membrane on the *cis* side to replenish. This can be due to large number of pores or large bulk volume so that it cannot quickly be replenished, a result of longer times for particle diffusion. Therefore, in membranes with a high pore density or a large *cis* chamber length, the separation of particles is determined by the difference of particle bulk drag coefficients (diffusion) rather than the particle-nanopore interaction. This is the reason P_{td} in Fig. 6(c) collapses into two bands, where the separation of particles with same charge

but different size (and drag coefficients) yields considerably higher P_{td} values than the separation of particles with the same size (same drag coefficient) but different charge. In other words, for sufficiently large fluid chambers and pore densities, the separation effectiveness has little to no dependency on membrane bias V_m (or charge) since membrane resistance becomes much less impactful than fluid resistance.

IV. CONCLUDING REMARKS

In this paper we examined the feasibility of using solid-state nanoporous membranes for separating nanoparticles by size and charge. The movement of individual spherical nanoparticles is modeled by using BD while the PNP approach is used to describe the electric potential landscape produced by the applied membrane bias or surface charge. The results of single-particle separation were then used in the continuum approach characteristic for macroscopic filtration process.

The cases that lead to best separation with nanoporous membranes were identified by calculating waiting times from simulations of two interacting particles of different size or charge. Particle separation effectiveness was determined by the maximum difference in the particle's translocation probability P_{td} , where large P_{td} implies a system that facilitates translocation for one particle species while impeding the other. We found that P_{td} was large in smaller nanopores no matter size or charge of the two particles investigated. However, smaller nanopores also increase the time it takes to separate the particles, t_{td} , which is not favorable for high-throughput filtration. The largest P_{td} 's with the smallest t_{td} 's for all pore sizes were produced for negatively charged particles of different sizes exposed to a positively biased membrane. In general, the particles of different sizes yielded larger separation probability difference than particles of different charges signifying that it is easier to separate beads by size rather than by charge.

We then considered how these results translate to macroscopic conditions. Using a continuum model to describe concentration of particles in the nanoporous membrane system, the values of maximum separation probabilities and

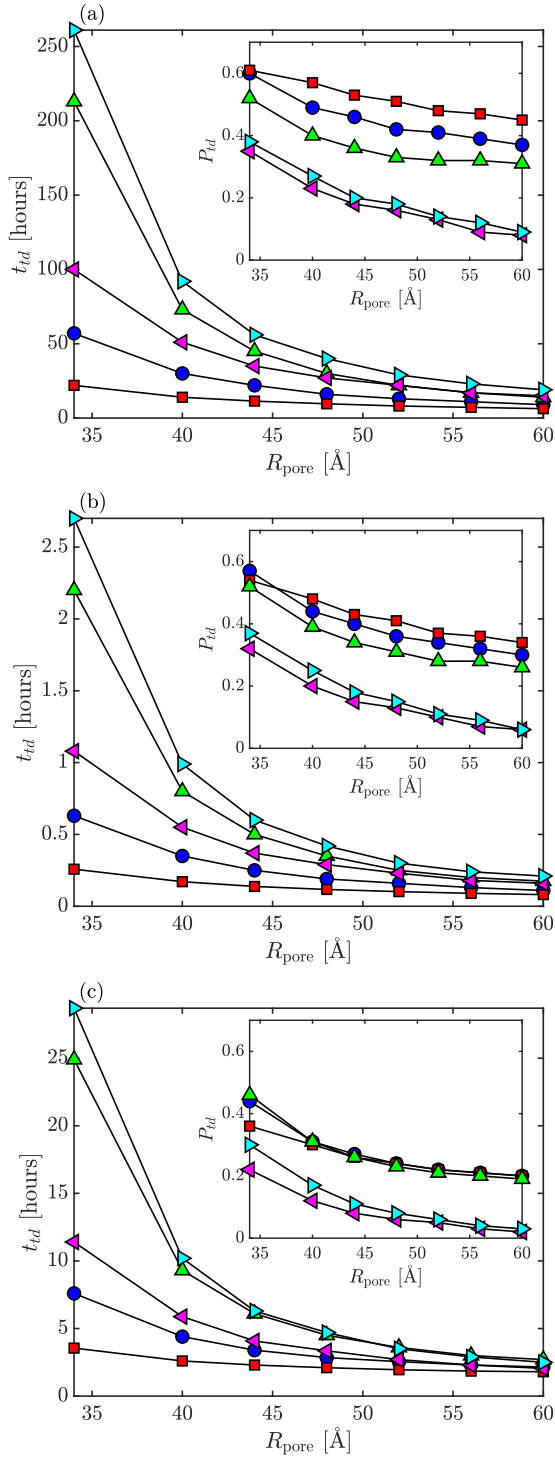


FIG. 6. Peak translocation probability difference time t_d and (inset) the maximum translocation probability difference P_d for a system where (◦) $R_1 = 10 \text{ \AA}$, $R_2 = 20 \text{ \AA}$, $q_i = 0$; (◻) $V_m = 1 \text{ V}$, $R_1 = 10 \text{ \AA}$, $R_2 = 20 \text{ \AA}$, $q_i = -5e$; (Δ) $V_m = -1 \text{ V}$, $R_1 = 10 \text{ \AA}$, $R_2 = 20 \text{ \AA}$, $q_i = -5e$; (\triangleleft) $V_m = 1 \text{ V}$, $q_1 = -5e$, $q_2 = 0$, $R_i = 20 \text{ \AA}$; (\triangleright) $V_m = -1 \text{ V}$, $q_1 = 0$, $q_2 = -5e$, $R_i = 20 \text{ \AA}$. P_d and t_d are calculated for systems scaled up to parameters (a) $N = 10^6 \text{ cm}^{-2}$, $W_1 = 0.1 \text{ mm}$, $W_2 = 10W_1$, (b) $N = 10^8 \text{ cm}^{-2}$, $W_1 = 0.1 \text{ mm}$, $W_2 = 10W_1$, and (c) $N = 10^8 \text{ cm}^{-2}$, $W_1 = 1 \text{ mm}$, $W_2 = 10W_1$.

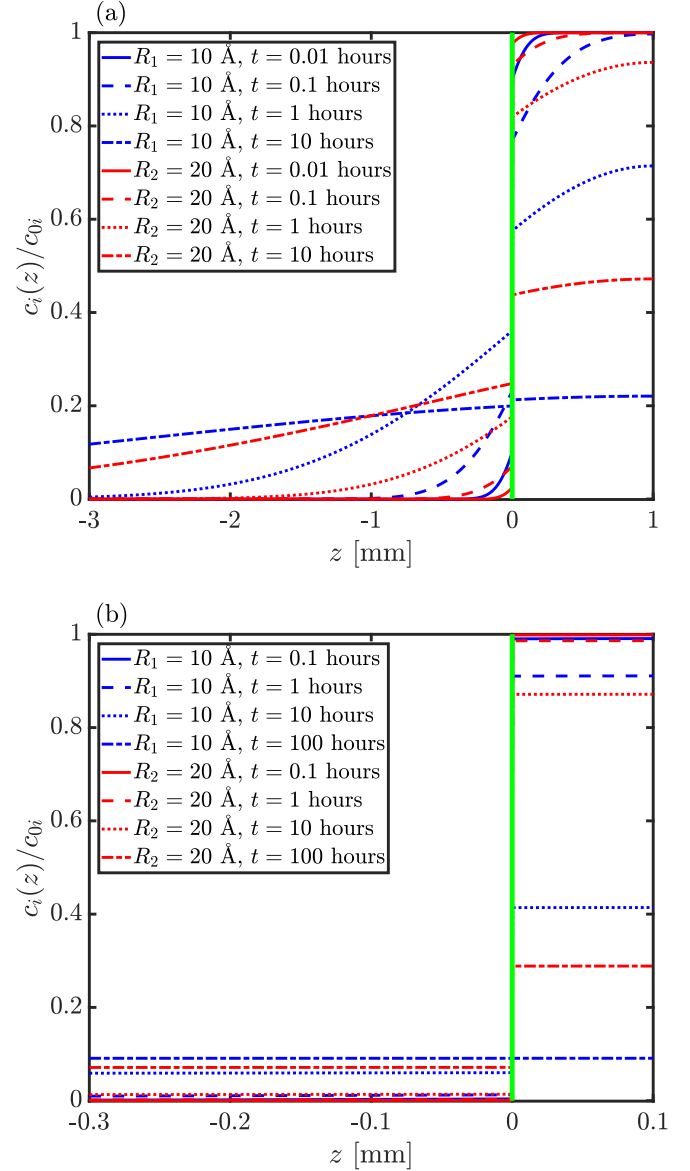


FIG. 7. Concentration profile in the z direction for $R_{\text{pore}} = 34 \text{ \AA}$, $V_m = 1 \text{ V}$, $R_1 = 10 \text{ \AA}$, $R_2 = 20 \text{ \AA}$, and $q_1 = q_2 = -5e$ at various times t . The macroscopic systems correspond to a higher-throughput filtration case where (a) $N = 10^8 \text{ cm}^{-2}$, $W_1 = 1 \text{ mm}$, $W_2 = 10W_1$ and a lower-throughput filtration case (b) $N = 10^6 \text{ cm}^{-2}$, $W_1 = 0.1 \text{ mm}$, $W_2 = 10W_1$. The vertical (green) line represents the location of the membrane at $z = 0 \text{ \AA}$.

times were calculated for systems of different sizes and pore densities. Utilizing smaller fluid chambers and low pore density led to the larger values of P_d than when the chamber size and/or pore density were large. Larger fluid chambers increase separation time, while decreasing separation effectiveness for each case studied; more porous membranes lead to lower separation times, but at the cost of decreasing P_d .

These results show that separating similar particles reliably may be viable but not a simple task. When trying to separate

similar particles, the first aspect to consider should be any size differences, as particle size is a dominating factor in determining fluid and membrane resistance. Particle charge differences should then be recognized since a membrane bias can be used to encourage or impede the translocation of specific particles. Even though electrostatic considerations may not increase effectiveness of charged particle separation notably in systems with larger chambers and/or more porous membranes, they can greatly decrease the separation time, a feature desired for high-throughput filtration of particles.

ACKNOWLEDGMENTS

This work was supported by the NSF through a CAREER Award No. DMR-1352218 (M.G.). We would like to acknowledge the use of Orion supercomputer at Clarkson University.

APPENDIX A

The electric potential distribution in the membrane and electrolyte solution is determined using the continuum approach. In this approach, the Poisson equation [39,40],

$$\nabla \cdot [\varepsilon(\mathbf{r})\nabla\phi(\mathbf{r})] = -\rho(\mathbf{r}), \quad (\text{A1})$$

is solved together with the Nernst-Plank equations,

$$\nabla \cdot [\mu_i C_i \nabla\phi + z_i D_i \nabla C_i] = 0, \quad i = \{K^+, Cl^-\}, \quad (\text{A2})$$

to determine the local concentrations of $C_{K^+}(\mathbf{r})$ and $C_{Cl^-}(\mathbf{r})$. For Eq. (A2), μ_i is the mobility of the i th species, $z_i = \pm 1$ depending on the charge of the ion, and $D_i = \mu_i k_b T / e$ is the diffusion coefficient.

The charge density $\rho(\mathbf{r})$ in Eq. (A1) is comprised of an electrolyte charge density, $\rho_e(\mathbf{r})$, and the membrane charge density, $\rho_m(\mathbf{r})$. These densities are described by

$$\rho_e(\mathbf{r}) = e\{C_{K^+}(\mathbf{r}) - C_{Cl^-}(\mathbf{r})\}, \quad (\text{A3})$$

and

$$\rho_m(\mathbf{r}) = \rho_{SiO_2}(\mathbf{r}), \quad (\text{A4})$$

where $\rho_{SiO_2}(\mathbf{r})$ is the surface charge density [41]. When solving the above system of equations, the electric potential difference is set to zero while ionic concentrations are set to the bulk values on the top and bottom boundaries in the z direction of the simulation domain. The membrane bias is held at V_m while the normal derivatives of the potentials and ionic fluxes on other boundaries are set to zero.

APPENDIX B

The following discussion focuses on how pore radius, membrane bias, and interparticle interaction affect the translocation process of spherical particles with different sizes and charges. The waiting time, t_w , is computed for two identical spherical beads of radii $R_{1,2} = 10 \text{ \AA}$, 15 \AA , and 20 \AA and electric charge of $q_{1,2} = -5e$ and 0 placed at random positions near a nanoporous membrane with different V_m and R_{pore} . An average waiting time ($\langle t_w \rangle$) for each case was calculated from production runs where two particles were simulated and then compared to simulations of only a single particle. In both cases the average waiting time was computed from ~ 2000

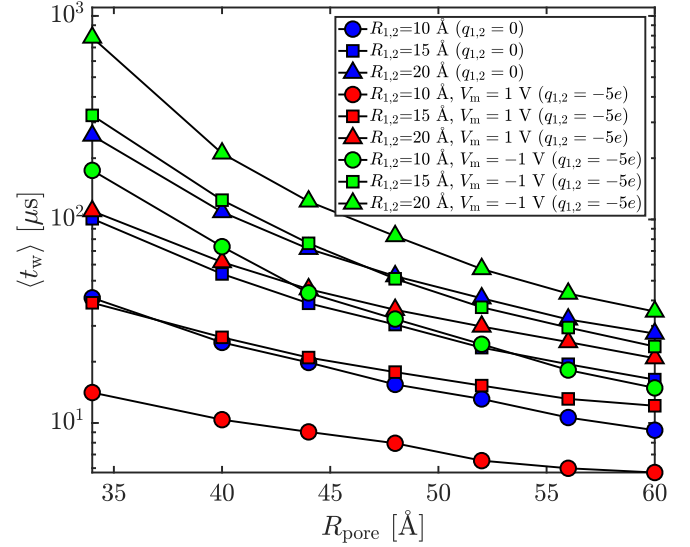


FIG. 8. Average waiting time ($\langle t_w \rangle$) from simulations of two identical and interacting spherical particles of various sizes and charges against pore radius R_{pore} for applied membrane biases $V_m = \pm 1$. Simulating an additional bead per simulation does not result in noticeable changes the waiting times observed.

translocations. For two-particle simulations, both beads are allowed to complete translocation and the waiting time for each bead is defined as the time from beginning of simulation to its successful translocation. We do this such that we do not consider the effects of increased particle density that occur when the simulation is stopped after one particle translocates.

Figure 8 shows that the longest waiting time, $\langle t_w \rangle = 810 \mu\text{s}$, is produced by the largest negatively charged particles in the smallest nanopore and a negative applied membrane bias ($R_i = 20 \text{ \AA}$, $q_{1,2} = -5e$, $V_m = -1$, $R_{\text{pore}} = 34 \text{ \AA}$). This is due to larger beads having a larger drag coefficient in addition to being less likely to find, enter, and then successfully translocate a small radius nanopore, a trend intensified when the effective pore radius is made smaller due to particle electric repulsion from the membrane surface [31,35,38]. For a particle of a given radius R_i , the waiting time decays as R_{pore} increases, however the particle's charge can greatly affect this trend as it changes the effective pore radius depending on the membrane's bias. For example, when R_{pore} decreases from 40-34 \AA while $R_i = 20 \text{ \AA}$, $\langle t_w \rangle$ increases by $\sim 270\%$ when $V_m = -1 \text{ V}$ and $q_{1,2} = -5e$, by $\sim 80\%$ when $V_m = 1 \text{ V}$ and $q_{1,2} = -5e$, and by $\sim 140\%$ when $q_{1,2} = 0e$.

A particle's charge affects its waiting time most notably for a nanopore with a smaller radius. This is seen in how the $\langle t_w \rangle$ values between the explored cases change from smaller pores with $R_{\text{pore}} = 34 \text{ \AA}$ to larger pores with $R_{\text{pore}} = 60 \text{ \AA}$ (Fig. 8). Waiting times for a bead moving through a smaller pore (with smaller $R_{\text{pore}}/R_{1,2}$ ratio) are mostly determined by the membrane bias and particle's charge, where $V_m = -1 \text{ V}$ and $q_{1,2} = -5e$ resulted in the longest time while $V_m = 1 \text{ V}$ and $q_{1,2} = -5e$ produce the shortest as seen in Fig. 8. This is because waiting times under these circumstances are greatly affected by the time required by a nanoparticle to find and enter the mouth of the nanopore, a task aided (or

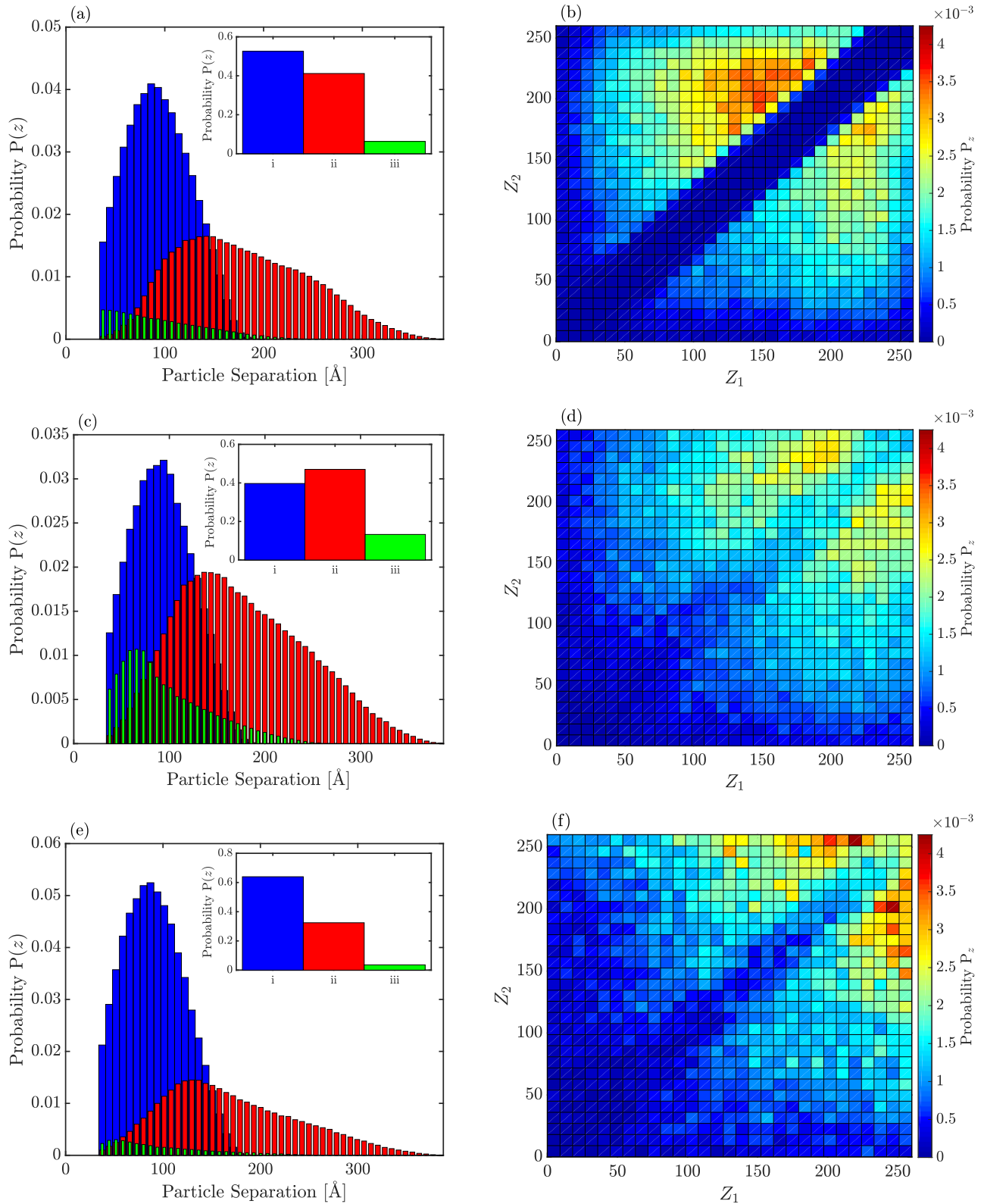


FIG. 9. Histograms of bead separation distance for when (i, blue) both beads are in the *cis* chamber, (ii, red) one bead is inside of the pore, (iii, green) both beads are in the pore for (a) $R_{\text{pore}} = 34 \text{ \AA}$, $V_m = 1 \text{ V}$, $R_{1,2} = 15 \text{ \AA}$, $q_{1,2} = -5e$; (c) $R_{\text{pore}} = 60 \text{ \AA}$, $V_m = 1 \text{ V}$, $R_{1,2} = 15 \text{ \AA}$, $q_{1,2} = -5e$; (e) $R_{\text{pore}} = 60 \text{ \AA}$, $V_m = -1 \text{ V}$, $R_{1,2} = 15 \text{ \AA}$, $q_{1,2} = -5e$. (inset) Probability histogram of the system's state. (b), (d), (f) Heatmap of two bead's z -coordinate center of mass position, $Z_{1,2}$, while both beads are located inside of the pore for (b) $R_{\text{pore}} = 34 \text{ \AA}$, $V_m = 1 \text{ V}$, $R_{1,2} = 15 \text{ \AA}$, $q_{1,2} = -5e$; (d) $R_{\text{pore}} = 60 \text{ \AA}$, $V_m = 1 \text{ V}$, $R_{1,2} = 15 \text{ \AA}$, $q_{1,2} = -5e$; (f) $R_{\text{pore}} = 60 \text{ \AA}$, $V_m = -1 \text{ V}$, $R_{1,2} = 15 \text{ \AA}$, $q_{1,2} = -5e$.

hindered) by an attraction (or repulsion) to the membrane surface.

For larger pores, having a slightly smaller effective pore opening due to surface charge effects is less impactful on the waiting time compared to when the pore is small. When $R_{\text{pore}} = 60 \text{ \AA}$, the particle charge affects translocation dynamics less than particle size, as seen by the small change in waiting times of similar bead sizes with different charges (Fig. 8). This results in the longest (shortest) waiting times corresponding to $R_{1,2} = 20 \text{ \AA}$ ($R_{1,2} = 10 \text{ \AA}$). In this case, the waiting time is mainly determined by the drag force on a nanoparticle, hence larger beads have the longest $\langle t_w \rangle$ regardless of their electric charge.

Waiting time simulations for single particles were also performed, yielding similar results seen in Fig. 8 where the waiting times were found to have a difference of $<10\%$ (most cases had $<4\%$ difference). This means the presence of two spherical beads in a nanoporous system does not result in notable additional hindrance of the translocation process compared to a single bead system. The largest difference in $\langle t_w \rangle$ between the cases shown is $R_{1,2} = 20 \text{ \AA}$, $q_{1,2} = -5e$, $V_m = -1 \text{ V}$, $R_{\text{pore}} = 34 \text{ \AA}$, which is also the case of the largest $\langle t_w \rangle$ for both models. However, even in this case the two bead simulations had lower waiting times only by $\sim 26 \mu\text{s}$ ($\sim 9\%$ difference compared to single bead simulations).

As the spherical nanoparticles we simulate interact with each other, we expected that a higher particle density of identical particles would lead to motion hindrance and an increase in waiting time. However, this was not clearly the case, so we look at the separation of the two $R_{1,2} = 15 \text{ \AA}$, $q_{1,2} = -5e$ particles throughout many simulations for $R_{\text{pore}} = 34 \text{ \AA}$, $V_m = 1 \text{ V}$ [Fig. 9(a)], $R_{\text{pore}} = 60 \text{ \AA}$, $V_m = 1 \text{ V}$ [Fig. 9(c)], and $R_{\text{pore}} = 60 \text{ \AA}$, $V_m = -1 \text{ V}$ [Fig. 9(e)]. Other beads and nanoporous membrane systems were also studied in this way, yielding similar results.

The particle separation distance histograms in Fig. 9 show three scenarios: both particles are outside of the nanopore, one particle is inside the pore, and both particles are inside of the pore. While both particles are outside of the nanopore, their separation distance obeys Gaussian distribution (with

cutoffs at the ends since the beads cannot move too closely to each other and their movement is confined to the bounding box) with a peak at $\sim 100 \text{ \AA}$ distance between particles. The peak particle separation when one bead is inside the nanopore ($\sim 130 \text{ \AA}$) is greater than that of when both particles are in the bulk, an expected result as the pore is longer than the size of the bounding box in the simulations. In this situation, the two particles rarely interact, save for when both are near the mouth of the pore (one inside, one outside), which occurs rarely. These trends are similar for all observed systems, however, the total probability of each state depends on the parameters as previously mentioned.

Both particles being located inside of the nanopore is the most interesting state since it forces interaction between the beads, however, it is also the least likely to occur. While both particles are inside of the nanopore, the histograms in Fig. 9 show that for the narrower pore, beads are most likely to be a minimum distance away from each other [Fig. 9(a)] has a peak at minimum separation). This is not the case for the wider pore, as the peak probability of separation occurs beyond the minimum separation [Fig. 9(c)].

To investigate further, we display the z -position probability (P_z) of each bead while both are inside the pore [Figs. 9(b), 9(d), and 9(f)]. For all cases explored, particularly for $V_m = -1 \text{ V}$, P_z is highest near the pore entrance ($z = 260 \text{ \AA}$), as expected since unsuccessful translocations of a single bead will most likely be near the mouth of the pore [35,49]. When $R_{\text{pore}} = 34 \text{ \AA}$ [Fig. 9(b)], the two particles do not occupy the same z -position, making a diagonal of $P_z \approx 0$, implying that one particle will not pass the other while inside the nanopore under these parameters. For the wider pore of $R_{\text{pore}} = 60 \text{ \AA}$, both beads tend not to stay at the same z position, however, $P_z > 0$ here indicating particles can pass each other in the nanopore. The additional radial space allows for particles in the pore to be further away from each other and pass each other, thus the shift in peak separation distance in Figs. 9(c) and 9(e). This also explains why two interactable bead simulations have a slightly shorter $\langle t_w \rangle$ when the effective pore radius is at its smallest (and beads are the largest), since a bead trying to escape the pore cannot pass another bead under those circumstances.

-
- [1] A. L. Garcia, L. K. Ista, D. N. Petsev, M. J. O'Brien, P. Bisong, A. A. Mammoli, S. R. Brueck, and G. P. López, *Lab Chip* **5**, 1271 (2005).
- [2] C. C. Striemer, T. R. Gaborski, J. L. McGrath, and P. M. Fauchet, *Nature (London)* **445**, 749 (2007).
- [3] P. Roy, T. Dey, K. Lee, D. Kim, B. Fabry, and P. Schmuki, *J. Am. Chem. Soc.* **132**, 7893 (2010).
- [4] J. Snyder, A. Clark Jr., D. Fang, T. Gaborski, C. Striemer, P. Fauchet, and J. McGrath, *J. Membr. Sci.* **369**, 119 (2011).
- [5] T. Z. Jubery, A. S. Prabhu, M. J. Kim, and P. Dutta, *Electrophoresis* **33**, 325 (2012).
- [6] M. E. Warkiani, A. A. S. Bhagat, B. L. Khoo, J. Han, C. T. Lim, H. Q. Gong, and A. G. Fane, *ACS Nano* **7**, 1882 (2013).
- [7] S. Howorka and Z. Siwy, *Chem. Soc. Rev.* **38**, 2360 (2009).
- [8] L. Wang, M. S. Boutilier, P. R. Kidambi, D. Jang, N. G. Hadjiconstantinou, and R. Karnik, *Nature Nanotechnol.* **12**, 509 (2017).
- [9] H. B. Park, J. Kamcev, L. M. Robeson, M. Elimelech, and B. D. Freeman, *Science* **356**, eaab0530 (2017).
- [10] L. Prozorovska and P. R. Kidambi, *Adv. Mater.* **30**, 1801179 (2018).
- [11] S. Mondal, I. M. Griffiths, and G. Z. Ramon, *J. Membr. Sci.* **588**, 117166 (2019).
- [12] M. E. Gracheva, J. Vidal, and J.-P. Leburton, *Nano Lett.* **7**, 1717 (2007).
- [13] J. Li, D. Stein, C. McMullan, D. Branton, M. J. Aziz, and J. A. Golovchenko, *Nature (London)* **412**, 166 (2001).
- [14] D. Fologea, B. Ledden, D. S. McNabb, and J. Li, *Appl. Phys. Lett.* **91**, 053901 (2007).

- [15] L. Movileanu, *Trends Biotechnol.* **27**, 333 (2009).
- [16] J. Larkin, R. Y. Henley, M. Muthukumar, J. K. Rosenstein, and M. Wanunu, *Biophys. J.* **106**, 696 (2014).
- [17] P. Waduge, R. Hu, P. Bandarkar, H. Yamazaki, B. Cressiot, Q. Zhao, P. C. Whitford, and M. Wanunu, *ACS Nano* **11**, 5706 (2017).
- [18] D. S. Talaga and J. Li, *J. Am. Chem. Soc.* **131**, 9287 (2009).
- [19] C. Plesa, S. W. Kowalczyk, R. Zinsmeister, A. Y. Grosberg, Y. Rabin, and C. Dekker, *Nano Lett.* **13**, 658 (2013).
- [20] J. Cervera, P. Ramírez, J. A. Manzanares, and S. Mafé, *Microfluid. Nanofluid.* **9**, 41 (2010).
- [21] M. Firmkes, D. Pedone, J. Knezevic, M. Doblinger, and U. Rant, *Nano Lett.* **10**, 2162 (2010).
- [22] L. Luo, S. R. German, W.-J. Lan, D. A. Holden, T. L. Mega, and H. S. White, *Annu. Rev. Anal. Chem.* **7**, 513 (2014).
- [23] M. Boukhet, F. Piguet, H. Ouldali, M. Pastoriza-Gallego, J. Pelta, and A. Oukhaled, *Nanoscale* **8**, 18352 (2016).
- [24] E. L. Bonome, F. Cecconi, and M. Chinappi, *Microfluid. Nanofluid.* **21**, 96 (2017).
- [25] G. Huang, K. Willems, M. Soskine, C. Wloka, and G. Maglia, *Nature Commun.* **8**, 935 (2017).
- [26] X. Qiu, H. Yu, M. Karunakaran, N. Pradeep, S. P. Nunes, and K.-V. Peinemann, *ACS nano* **7**, 768 (2013).
- [27] D. P. Hoogerheide, P. A. Gurnev, T. K. Rostovtseva, and S. M. Bezrukov, *Biophys. J.* **114**, 772 (2018).
- [28] M. Muthukumar, *J. Chem. Phys.* **141**, 081104 (2014).
- [29] W. Si and A. Aksimentiev, *ACS Nano* **11**, 7091 (2017).
- [30] I. Jou and M. Muthukumar, *Biophys. J.* **113**, 1664 (2017).
- [31] C. C. Wells, D. V. Melnikov, and M. E. Gracheva, *J. Chem. Phys.* **150**, 115103 (2019).
- [32] S. K. Kannam, S. C. Kim, P. R. Rogers, N. Gunn, J. Wagner, S. Harrer, and M. T. Downton, *Nanotechnology* **25**, 155502 (2014).
- [33] A. Ammenti, F. Cecconi, U. Marini Bettolo Marconi, and A. Vulpiani, *J. Phys. Chem. B* **113**, 10348 (2009).
- [34] F. Cecconi, M. Bacci, and M. Chinappi, *Protein Pept. Lett.* **21**, 227 (2014).
- [35] I. A. Jou, D. V. Melnikov, and M. E. Gracheva, *Nanotechnology* **27**, 205201 (2016).
- [36] Z. Liu, X. Shi, and H. Wu, *Nanotechnology* **30**, 165701 (2019).
- [37] A. Nadtochiy, D. Melnikov, and M. Gracheva, *ACS Nano* **7**, 7053 (2013).
- [38] I. A. Jou, D. V. Melnikov, A. Nadtochiy, and M. E. Gracheva, *Nanotechnology* **25**, 145201 (2014).
- [39] A. Nikolaev and M. E. Gracheva, *J. Comput. Electron.* **13**, 818 (2014).
- [40] A. Nikolaev and M. E. Gracheva, *Nanotechnology* **22**, 165202 (2011).
- [41] C. C. Wells, I. A. Jou, D. V. Melnikov, and M. E. Gracheva, *J. Chem. Phys.* **144**, 104901 (2016).
- [42] C. C. Wells, D. V. Melnikov, and M. E. Gracheva, *J. Chem. Phys.* **147**, 054903 (2017).
- [43] D. L. Ermak and J. McCammon, *J. Chem. Phys.* **69**, 1352 (1978).
- [44] N. Watari, M. Doi, and R. G. Larson, *Phys. Rev. E* **78**, 011801 (2008).
- [45] P. Dechadilok and W. M. Deen, *Ind. Eng. Chem. Res.* **45**, 6953 (2006).
- [46] M.-m. Kim and A. L. Zydney, *J. Colloid Interface Sci.* **269**, 425 (2004).
- [47] A. W. C. Lau and T. C. Lubensky, *Phys. Rev. E* **76**, 011123 (2007).
- [48] A. Gubbiotti, M. Chinappi, and C. M. Casciola, *Phys. Rev. E* **100**, 053307 (2019).
- [49] Z. K. Hulings, D. V. Melnikov, and M. E. Gracheva, *Nanotechnology* **29**, 445204 (2018).